

Acoustic Shock Emission in a Collision of a Drop with Water Surface

V. E. Prokhorov*

Ishlinsky Institute for Problems in Mechanics RAS, Moscow, 119526, Russia

*Corresponding Author: V. E. Prokhorov. Email: prohorov@ipmnet.ru

Received: 31 October 2019; Accepted: 08 March 2020

Abstract: The collision of droplets with a water surface is being actively developed in the interests of many applied problems—transfer of matter through the ocean-atmosphere boundary, underwater acoustic noise of the marine environment, measurement of precipitation intensity, various technologies, and much more. One of the research priorities is acoustic radiation, in particular, shock sound arising at the moment a drop contacts the surface. The impact of the drop is preceded by processes that affect the shape of the drop, because of which it noticeably deviates from the spherical one. As a result, the final (contact) velocity changes—one of the most important parameters of collision. The study of the listed factors is carried out in this work by means of broadband acoustic measurements and high-speed video recording.

Keywords: Droplet; impact; acoustic emission; shape; final velocity; cross-correlation

1 Introduction

Collision of a droplet with a free surface of a liquid is accompanied by acoustic emission, the radiation mechanisms of which differ significantly from the processes that occur when a droplet hits a solid surface. In a liquid, in contrast to a solid, at a late stage of collision—several tens of milliseconds after contact—resonant sound packets emitted by air bubbles emerging from the underwater cavity appear [1,2]. Bubble formation occurs due to the air drawn in by the drop at the moment of collision [3]. This type of radiation is detected confidently, but its key parameters (frequency, amplitude, duration) do not repeat from experiment to experiment [4]. The initial shock impulse is much more stable under constant experimental conditions [5], however, fluctuations are also observed in it, mainly due to deformations of the bottom of the droplet and the water surface immediately before the collision [6]. The collision scenario is largely determined by the final shape of the drop, which the drop takes due to oscillations. The number of oscillations and the final phase depend on the method of formation, separation, and height of incidence. A significant contribution is made by the internal flows of the droplet, the intensity and geometry of which can change in the presence of an external electric field [7], or due to rapid change in the droplet temperature during the fall [8]. One may try to take into account the effects of deformation by replacing spherical droplets with regular spheroids [9], but in reality, as fine experiments [10] show, deformation is extremely local and is concentrated in the very small bottom segment of the drop. The nature of the deformation—the formation of an air cushion, distorting the shape of the bottom of the drop and the underlying surface



This work is licensed under a Creative Commons Attribution 4.0 International License, which permits unrestricted use, distribution, and reproduction in any medium, provided the original work is properly cited.

itself. Under the assumption of vertical symmetry of the deformation and at small Reynolds numbers, a numerical simulation of the air gap based on the viscous lubrication theory [11] gives results comparable to the experiment [10,12].

Under conditions of flow symmetry, it would be possible to establish the impact velocity and determine the effective impact pressure. However, in reality, at the time of the splashdown, the droplet shape is noticeably different from spherical—most often it is an irregular ovoid with an arbitrarily oriented main axis [13].

For this reason, a theoretical estimation of the droplet impact pulse is fully possible if the droplet has the shape of an ideal sphere [14] or a regular spheroid [9].

In references, the main factors determining the interaction of a droplet with a surface include the collision velocity and droplet diameter. However, both parameters are considered separately without interconnection with each other. To a certain extent, this is justified for small droplets (<2 mm), whose shape is close to spherical. Larger droplets oscillate in shape during movement, and by the time of contact acquire the form of an irregular ovoid. Depending on the type of ovoid—prolate or oblate—the collision speed can noticeably change.

One may list many effects in which the final shape of the droplet plays a significant role. Among them, the formation of a splash structure—to reduce the shape influence and even eliminate it, they try to make droplets as little as possible [15]. The efficiency of transfer of droplet matter into the atmosphere and the formation of secondary droplets upon impact with a wetted surface [16,17], also depends on the shapes of the impacting drops.

A large number of works are devoted to the collision of a droplet with a solid surface, when a droplet shape distortion at the contact is many times greater than the oscillation magnitude of the shape of the falling droplet [18,19]. The influence of the droplet shape was investigated in connection with the capture of air and the subsequent formation of underwater resonant cavities [20]. At the same time, the inverse effect of air on the final droplet shape is not considered significant according to experiments [21] and numerical calculations [22].

Among the many references, it is hard to find one indicating droplet deformation as a factor of influence on the impact velocity, which, in turn, determines to some extent the amplitude of the shock acoustic pulse. In this work, the relationship between the velocity and shape of the droplet is considered in the context of their influence on the acoustic shock pulse.

We consider a practically important case—the distribution of the shock field of pressure inside the liquid on a vertical line, which is a continuation of the drop moving line, since with this geometry the theory allows direct experimental verification by routine measurements [6,23]. Although a single drop is considered here, the results can be transferred to processes in which multiple drops are involved—rain or technological processes, for example, shear stresses in cross-junction devices [24].

2 Theoretical Background

The mechanism of shock radiation, as in the case of a collision with a solid surface, is of kinematic nature: the radiation comes from a contact contour (Fig. 1) of a radius r_e that expands at the initial stage with supersonic speed [25–29]. The supersonic stage ceases at the moment $t_c = aM/2c$ from the initial contact when the radius of the contact spot reaches $r_c = aM$; $M = U/c$ —Mach number c —sound velocity in the water.

At the moment t the acoustic field on the axis z (line of incidence of the droplet) at point M located at a distance R_e from the contact contour, determined by the signal emitted at the moment $(t - R_e/c)$ when

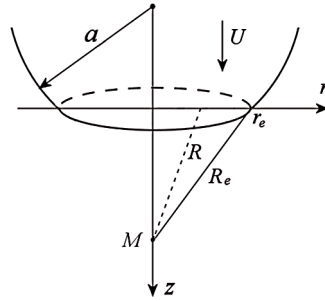


Figure 1: Geometry scheme of the contact between drop and water surface. a – radius of the drop, U – final (contact) velocity, r_e – radius of the expanding contact contour

contour radius is $r_e = \sqrt{2aU(t - R_e/c)}$. Along with $R_e^2 = z^2 + r_e^2$ this yields quadratic equation for R_e of which the solution is

$$R_e = aM \left(\sqrt{1 + t' + z'^2} - 1 \right) = r_c \left(\sqrt{1 + t' + z'^2} - 1 \right) \quad (1)$$

where $t' = t/t_c$, $z' = z/r_c$.

Next, we take the equation of sound propagation in the form $\nabla^2 \varphi - c^{-2} \partial^2 \varphi / \partial t^2 = 0$ where φ is the velocity potential. On surface $z = 0$ the following conditions are satisfied:

$$\varphi(r, 0, t) = 0, \quad \varphi_z(r, t) = 0 \text{ at } r > r_e \text{ (the liquid is undisturbed outside the contact contour);}$$

$$\varphi_z(r, 0, t) = u(t) \text{ at } r < r_e \text{ (inside the contour, speed is finite);}$$

$$\varphi_z(R_e, 0, t) = U \text{ at } r = r_e \text{ (on the contour itself, the speed equals the contact speed)}$$

Initial condition has a simplest form and means that no acoustic field is earlier than impact:

$$\varphi(r, z, 0) = 0, \quad \varphi_z(r, z, 0) = 0.$$

Standard solution [30] yields velocity potential at point M of z -axis (Fig. 1):

$$\varphi(z, t) = -\frac{1}{2\pi} \iint_S \frac{\varphi_z(r, t - R/c)}{R} r dr d\theta = -\int_z^{R_e} u(r, t - R/c) dR \quad (2)$$

Accordingly, the sound pressure at depth z at the moment t is

$$p = -\rho \frac{\partial \varphi}{\partial t} = \rho \left(\int_z^{R_e} \frac{\partial u(t - R/c)}{\partial t} dR + \frac{\partial R_e}{\partial t} U \right) \quad (3)$$

Assuming that the velocity u is constant over the entire contact surface, i.e., $\partial u / \partial t = 0$ we get from (1–3)

$$p = \frac{\rho U c}{\sqrt{1 + t' + z'^2}} \quad (4)$$

Expression (4) is a simplified notation of [14] at $M \ll 1$.

3 Experimental Apparatus

Experiments were carried out at “ESP” – laboratory stand from the “Hydrophysical Complex IPMech RAS” [31]. Drop of diameter $D = 2a$ fall from the dispenser located at some height H . For video recording

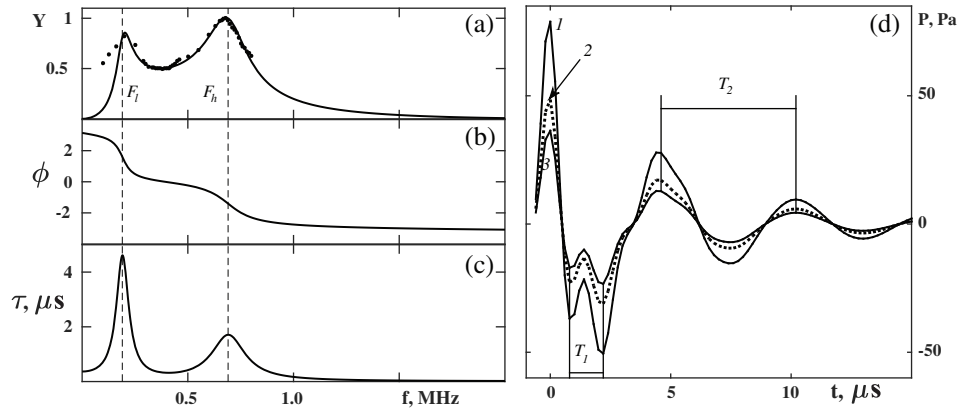


Figure 2: Magnitude (a) and phase (b) response, and delay time (c) of the synthesized hydrophone. Dots in a – real frequency response characteristic according to certificate [48796-11: GI800 Hydrophones]. d – responses of the synthesized hydrophone to signal (4) at $D = 5, 3, 2$ mm (1, 2, 3), $U = 5$ m/s, $z = 3$ cm

camera Optronis CR3000x2 [32] was used. The acoustic pressure was measured by hydrophone GI800-13 [33], whose performance data along with testing output signals are given in Fig. 2.

Ideal hydrophone (curves in Figs. 2a–2c) has been synthesized as Chebyshev Type I bandpass filter [34] fitting the real magnitude response (dot plot in Fig. 2a).

In Fig. 2d hydrophone outputs simulate input (4) for the three diameters of drops falling at the same velocity. All the curves are similar, they differ only by amplitudes. One may see two character periods $T_1 = 1.4 \cdot 10^{-6}$ and $T_2 = 5.6 \cdot 10^{-6}$ s which are conditioned by two resonant peaks at low and high frequencies $F_l = 180$ and $F_h = 700$ kHz (Fig. 2a). Also we can see that process of long period T_2 is delayed about $5 \mu\text{s}$ (see Fig. 2c) while short period signal T_1 delayed only for less than $2 \mu\text{s}$ (see Fig. 2c) and phase inverted (see Fig. 2b). All this features are associated with the intrinsic properties of the hydrophone and are not related to the impacts and should be excluded from experimental data.

The hydrophone introduces noticeable distortion into the measurement of an extremely high-frequency shock pulse. Estimates showed that the introduced attenuation when measuring the amplitudes of fast pressure pulses, like shock, is characterized by a factor of about 0.15.

4 Experimental Results

4.1 Shock Impulse Attenuation with Depth

At a constant height of incidence, the speed of the drop is maintained approximately constant except for some fluctuations caused by oscillations of the droplet shape.

Major variability should be expected from the denominator of (4). If we represent (4) in dimensional form $p = \frac{\rho U^2 a}{\sqrt{a^2 M^2 + 2aUt + z^2}}$ then, at natural drops falling velocities ($M \ll 1$), sufficient depth ($z \gg a$), and taking into account the correction coefficient, expression (4) turns to

$$p = 0.15 \cdot \rho U^2 a / z \quad (5)$$

It follows from (5) that factors leading even to small deviations in the final velocity will cause noticeable fluctuations in acoustic pressure. Most of all, this may effect at low speed range.

On Fig. 3a, the dots show the experimental dependence into which the curve (5) fits well. Note that the velocity pulsates relative to the average value, which is noticeably less than the $U = \sqrt{2gH}$ (Fig. 3b).

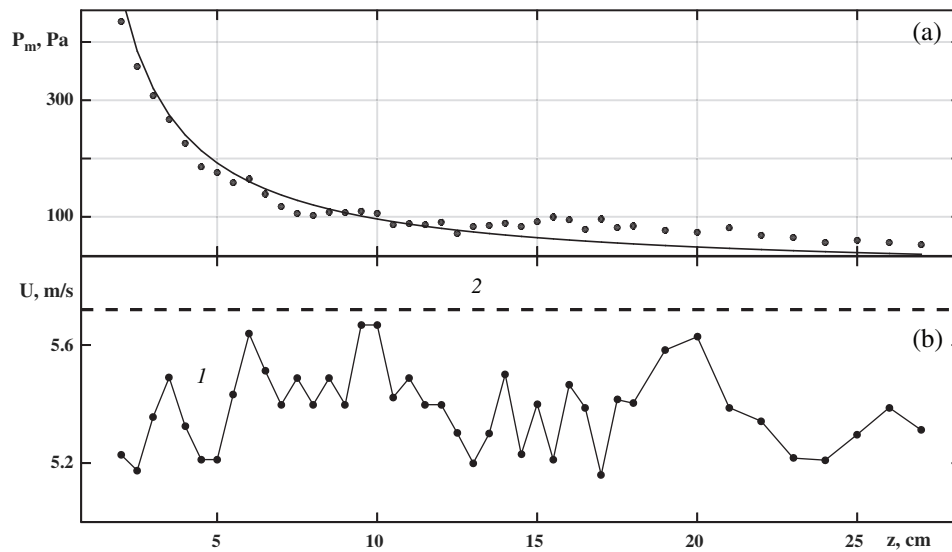


Figure 3: *a* – The amplitude of the shock pulse P_m depending on the depth z of the hydrophone. Dots – experiment, solid is theoretical approximation (5). *b* – Impact velocity: 1 – measured from videoframes, 2 – $U = \sqrt{2gH}$. $H = 1.65$ m

Fluctuations in the experimental graph against the curve are associated with oscillations in the impact velocity (Fig. 3b) caused by instability of the shape of the droplet during the fall.

In this case, the height of the fall remained constant, so the variability of the form is largely due to secondary factors—flows in the ambient air and instability of the separation scenario. So, the shape of the splashed drop is unstable that can be characterized by ratio $e = A/B - 1$ (Fig. 4) which will be referred to below as *e*-ratio. Fig. 4 shows how the *e*-ratio changed in each experiment. The depth of the hydrophone is plotted along the abscissa—it serves as the number of the experiment. It is seen that, with an increase in depth to 15 cm, the drop, while remaining slightly oblate, gradually acquired a shape close to a sphere. In this case, the peak pressure amplitude (dots) followed the theoretical curve (Fig. 3). However, then ($z > 15$ cm) the drop shape sharply returns to the oblate form; this is accompanied by a noticeable deviation of the experimental points from the solid curve in Fig. 3. Below we consider the functions of cross-correlation of speed and *e*-ratio, so the question will be clarified.

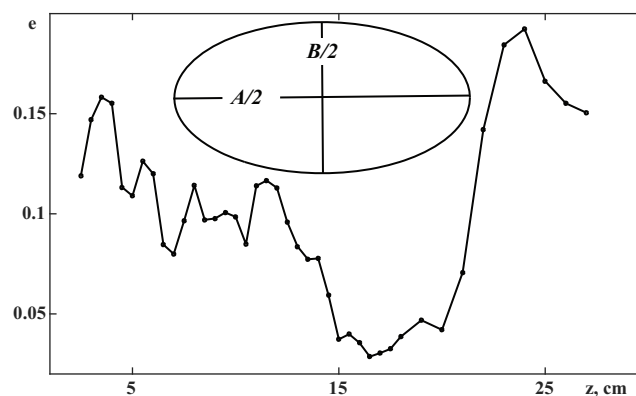


Figure 4: The variability of the ratio $e = A/B - 1$. Insert: sketch of equivalent ovoidal drop

4.2 Effect of Variability of the Drop Shape

The variability of the height of the fall is the main factor affecting the shape of the impacting drop. In the process of falling, the drop makes a series of shape oscillations and, by the time of contact, usually has the form of an irregular ovoid. Even slight variations in height lead to noticeable changes in shape. In Fig. 5 drops falling from the heights of 112 and 120 cm, at the moment of contact sharply differ in shape being respectively, oblate and prolate. A significant increase in height to 167 cm leads to a sharp change in shape—it becomes significantly irregular (Fig. 5, photo 3).

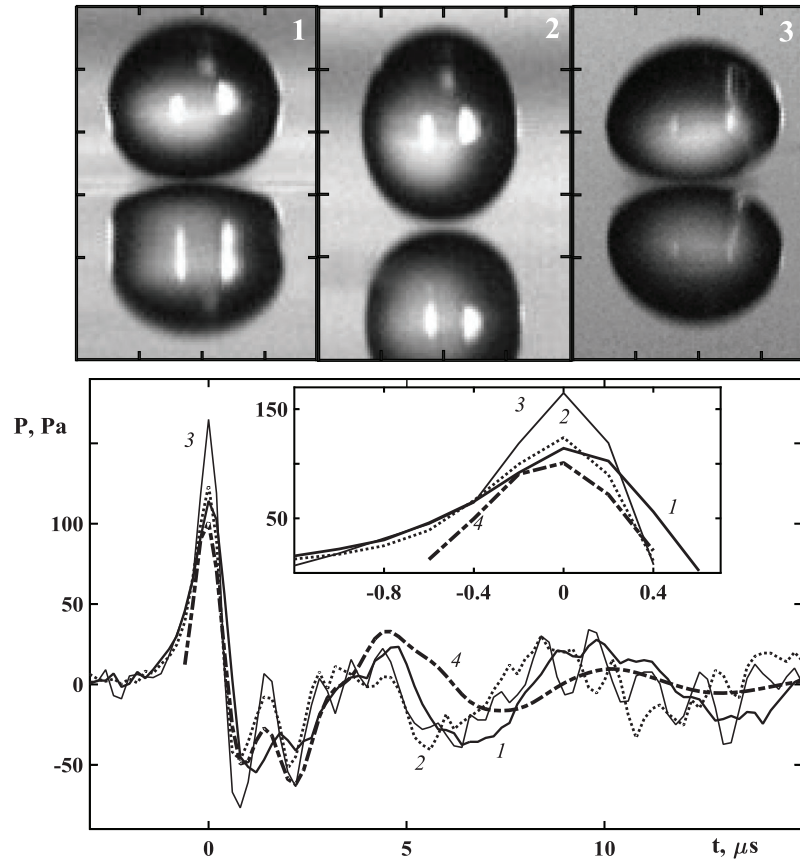


Figure 5: Snap-shots of the drops right before the contact and plots of hydrophone responses. Numberings of the images and curves are identical. 1, 2, 3: $H = 112, 122, 167$ cm. 4 – calculation in accordance with (5) at $H = 115$ cm. Insert: enlarged fragment around vertex of the shock. Time (μs) is counted from shock maximum. Tick mark interval in the frames is 2 mm

Impact pressure data (curves 1 and 2, Fig. 5) are obtained at the hydrophone depth 3 cm, as well as theoretical plot 4, and at adjacent heights of fall providing final velocity about 4.5 m/s. Curve 3 corresponds to depth more than twice as large ($z = 6.5$ cm), however, the height of its fall is one and a half times more (final speed 5.7 m/s). Despite attenuation due to double deepening, the shock pulse # 3 turns out to be 1.5 times more due to the higher speed.

Acoustic pressure plots 1–3 manifests the same features of hydrophone that were previously noted in test signals (Fig. 2d). With a delay of about $1.5 \mu\text{s}$, an inverted double-peak signal (period T_1) arises due to resonance at a frequency of F_h (Fig. 2a), and about $5 \mu\text{s}$ later low-frequency (period T_2) oscillations start

due to a resonance at a frequency of F_l (Fig. 2a). Of course, all of the above features are repeated in the theoretical curve 4 that corresponds to expression (5).

A drop falling from a constant height performs a finite number of shape oscillations before a collision. When the experiments are repeated many times, among the many splashdown scenarios, there is the most probable one in which a certain droplet shape occurs most often. With a changing fall height, such a scenario does not exist. The drop takes the form determined, first of all, by the final phase of the oscillations, as well as by random factors caused by instability of the environment. The shape of the drop affects the final velocity and, accordingly, the amplitude of the shock pulse (4). In the gap between an oblate drop and the surface, the air cushion has a larger surface than one in the case of a prolate drop. Therefore, the air exchange in oblate drop cushion will take a longer time; it should be expected that oblate drop will be decelerated in more extent than prolate drop.

The frames of splashed drops obtained in the experiment with a successive increase in the height of fall with a step of 5 cm are shown in Fig. 6. Among the ten fragments, not one in which the droplet shapes were similar.

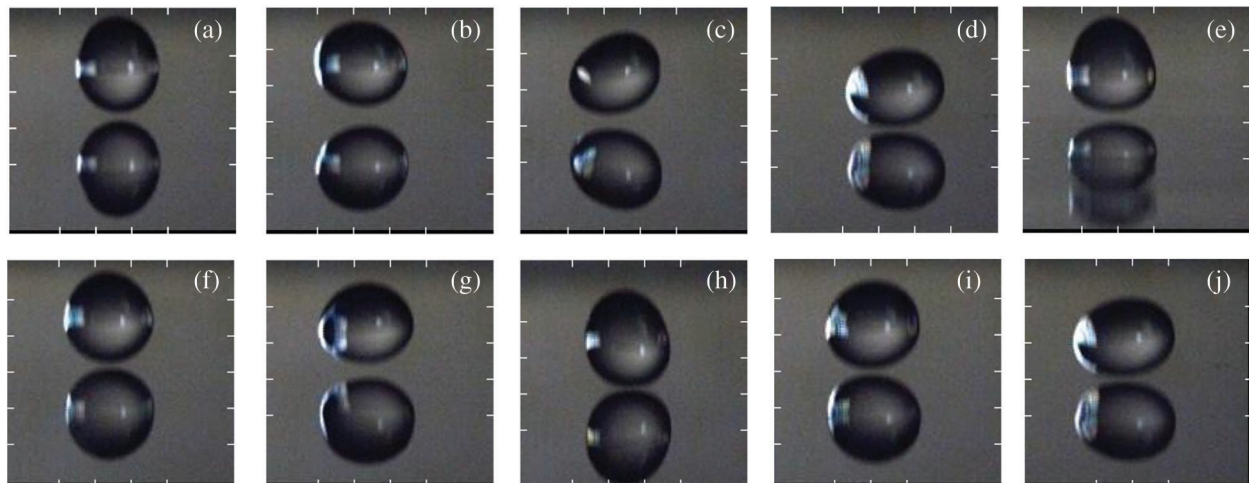


Figure 6: Drops right before splash-down. Lower “drops” are reflections. $a-j$: $H = 122-167$ through 5 cm. Tick mark interval – 2 mm

Along with the height of the fall, the impact velocity also increases, the variability of which is shown in Fig. 7a. Its values (dots) are grouped above and below the smoothing curve 2 and generally lie noticeably below the canonical level $\sqrt{2gH}$.

Fig. 7b shows a plot of the e -ratio as a function of height. It can be noted that the local extrema of the e - and U -curves are in antiphase. This becomes apparent if we compare the dependencies $U' = U - \langle U \rangle$ and $e' = e - \langle e \rangle$, where the symbol $\langle \rangle$ means the smoothing operation. Both dependences are plotted on the same abscissa axis (Fig. 7c); it can be seen that they are in sharp antiphase.

The picture is supplemented by the cross-correlation coefficient of both quantities $R_{eu} = \frac{\mu[(e - \mu(e))(U - \mu(U))]}{\sigma_e \sigma_U}$, where $\mu()$ is the mathematical expectation, σ – the square root of the variance. The form of the coefficient (Fig. 8) indicates that the sequences $e - \mu(e)$ and $U - \mu(U)$ are in antiphase, i.e., an increase in e -ratio leads to a decrease in speed. In other words, a prolate drop, under equal conditions, has a greater final speed than an oblate drop.

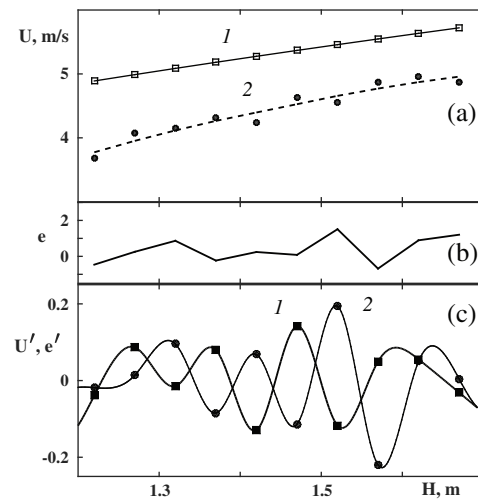


Figure 7: Plots vs. height: *a*–Final velocity: 1 – $U = \sqrt{2gH}$, dots–measured from videorecords (2 – smoothed), *b* – *e*-ratio (see Fig. 4), *c* – detrended and smoothed velocity 1 and *e*-ratio 2

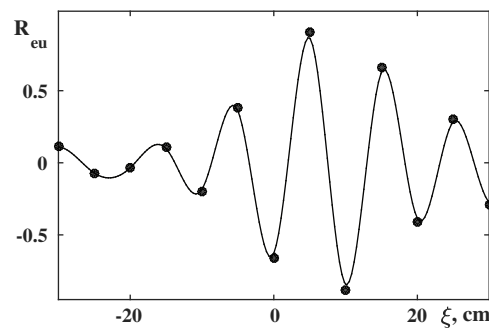


Figure 8: Cross-correlation coefficient between final velocity and *e*-ratio

5 Conclusion

The acoustic impulse arising from the impact of a drop on a water surface is characterized by an extremely short lifetime. Because of the bounded bandwidth, present-day hydrophones do not quite satisfy the requirements of adequate reproduction of the initial shock pulse. This mainly affects the appearance of spurious components in the output signal, which are associated with the intrinsic properties of hydrophones. Nevertheless, acoustic sensors together with modern video cameras allow us to establish important features of the collision process and their influence on the amplitude of the shock pulse. In these experiments, it was revealed:

1. When a drop falls from a constant height, the decay of the shock pulse with depth is characterized by noticeable deviations from the canonical dependence followed by velocity fluctuations, and accompanied by variations in the *e*-ratio.

2. The influence of the shape of the splashed drop on the collision velocity was confirmed in experiments with a varying drop height. Cross-correlation processing of geometric parameters and velocity of the droplet revealed a direct relationship between the final velocity and the droplet shape.

Funding Statement: The work was supported by the Russian Science Foundation (Project 19-19-00598 “Hydrodynamics and energetics of drops and droplet jets: formation, motion, break-up, interaction with

the contact surface”), <https://www.rscf.ru/>. Experiments were carried out at “ESP” stand from USF “HPC IPMech RAS”.

Conflicts of Interest: The author declare that he has no conflicts of interest to report regarding the present study.

References

1. Prosperetti, A., Oguz, H. (1993). The impact of drops on liquid surfaces and the underwater noise of rain. *Annual Review of Fluid Mechanics*, 25(1), 577–602. DOI 10.1146/annurev.fl.25.010193.003045.
2. Bjomo, L. (1994). Underwater rain noise: sources, spectra and interpretations. *Journal De Physique IV. Colloque C5. Supplement au Journal de Physique* 3, 4, C5-1023–C5-1030.
3. Oguz, H., Prosperetti, A. (1990). Bubble entrainment by the impact of drops on liquid surfaces. *Journal of Fluid Mechanics*, 219, 143–179. DOI 10.1017/S0022112090002890.
4. Chashechkin, Y., Prokhorov, V. (2017). Acoustics and hydrodynamics of a drop impact on a water surface. *Acoustical Physics*, 63(1), 33–44. DOI 10.1134/S10637711016060038.
5. Pumphrey, H. (1991). Underwater rain noise—the initial impact component. *Proceedings of the UK Institute of Acoustics*, 13, 192–200.
6. Prokhorov, V. (2018). Influence of molecular effects on the emission of sound in a low-velocity impact of a drop on water surface. *Journal of Experimental and Theoretical Physics*, 126(4), 479–484. DOI 10.1134/S1063776118030184.
7. Esmaeeli, A., Behjatian, A. (2017). A note on the transient electrohydrodynamics of a liquid drop. *Fluid Dynamics & Materials Processing*, 13(3), 143–153.
8. Wang, Z., Dong, K., Zhan, S. (2017). Numerical analysis on unsteady internal flow in an evaporating droplet. *Fluid Dynamics & Materials Processing*, 13(4), 221–234.
9. Howe, M., Hagen, N. (2011). On the impact noise of a drop falling on water. *Journal of Sound and Vibration*, 330(4), 625–635. DOI 10.1016/j.jsv.2010.08.038.
10. Tran, T., de Maleprade, H., Sun, C., Lohse, D. (2013). Air entrainment during impact of droplets on liquid surfaces. *Journal of Fluid Mechanics*, 726, R3. DOI 10.1017/jfm.2013.261.
11. Leal, L. (1992). *Laminar flow and convective transport processes*. Boston: Butterworth-Heinemann.
12. Hendrix, M., Bouwhuis, W., van der Meer, D., Lohse, D., Snoeijer, J. (2016). Universal mechanism for air entrainment during liquid impact. *Journal of Fluid Mechanics*, 789, 708–725. DOI 10.1017/jfm.2015.757.
13. Chashechkin, Y., Prokhorov, V. (2016). Primary acoustic signal structure during free falling drop collision with a water surface. *Journal of Experimental and Theoretical Physics*, 122(4), 748–758. DOI 10.1134/S1063776116020175.
14. Guo, Y., Williams, J. (1991). A theoretical study on drop impact sound and rain noise. *Journal of Fluid Mechanics*, 227, 345–355. DOI 10.1017/S0022112091000149.
15. Leng, L. (2001). Splash formation by spherical drops. *Journal of Fluid Mechanics*, 427, 73–105. DOI 10.1017/S0022112000002500.
16. Hobbs, P., Osheroff, T. (1967). Splashing of drops on shallow liquids. *Science*, 158(3805), 1184–1186. DOI 10.1126/science.158.3805.1184.
17. Cossali, G., Coghe, A., Marengo, M. (1997). The impact of single drop on a wetted solid surface. *Experiments in Fluids*, 22(6), 463–472. DOI 10.1007/s003480050073.
18. Thoroddsen, S., Sakakibara, J. (1998). Evolution of the fingering pattern of an impacting drop. *Physics of Fluids*, 10(6), 1359–1374. DOI 10.1063/1.869661.
19. Mundo, C., Sommerfeld, M., Tropea, C. (1995). Droplet-wall collisions: experimental studies of the deformation and breakup process. *International Journal of Multiphase Flow*, 21(2), 151–173. DOI 10.1016/0301-9322(94)00069-V.
20. Pumphrey, H., Elmore, P. (1990). The entrainment of bubbles by drop impacts. *Journal of Fluid Mechanics*, 220, 539–567. DOI 10.1017/S0022112090003378.

21. Thoroddsen, S. (2002). The ejecta sheet generated by the impact of a drop. *Journal of Fluid Mechanics*, 451, 373–381. DOI 10.1017/S0022112001007030.
22. Yarin, A., Weiss, D. (1995). Impact of drops on solid surfaces: self similar capillary waves, and splashing as a new type of kinematic discontinuity. *Journal of Fluid Mechanics*, 283, 141–173. DOI 10.1017/S0022112095002266.
23. Franz, G. (1959). Splashes as sources of sounds in liquids. *Journal of the Acoustical Society of America*, 31(8), 1080–1096. DOI 10.1121/1.1907831.
24. Chekifi, T. (2019). Droplet breakup regime in a cross-junction device with lateral obstacles. *Fluid Dynamics & Materials Processing*, 15(5), 545–555. DOI 10.32604/fdmp.2019.01793.
25. Dergarabedian, P. (1955). Compressibility effect during water entry. *NAVORD Report 3253*, California, USA.
26. Heymann, F. (1969). High speed impact between a liquid drop and a solid surface. *Journal of Applied Physics*, 40 (13), 5113–5122. DOI 10.1063/1.1657361.
27. Field, J. (1991). The physics of liquid impact, shock wave interactions with cavities, and the implications to shock wave lithotripsy. *Physics in Medicine & Biology*, 36(11), 1475–1484. DOI 10.1088/0031-9155/36/11/007.
28. Lee, M., Longoria, R., Wilson, D. (1997). Ballistic waves in high-speed water entry. *Journal of Fluids and Structures*, 11(7), 819–844. DOI 10.1006/jfls.1997.0103.
29. Field, J., Camus, J., Tinguely, M., Obreschkow, D., Farhat, M. (2012). Cavitation in impacted drops and jets and the effect on erosion damage thresholds. *Wear*, 290–291, 154–160. DOI 10.1016/j.wear.2012.03.006.
30. Morse, P. (1948). *Vibration and sound*. New York: McGraw-Hill Book Company Inc.
31. USF “HPC IPMech RAS”. (2018). Unique science facility “Hydrophysical complex for modeling of hydrodynamic processes in the environment and their impact on underwater technical objects, as well as the transport of impurities in the ocean and atmosphere”. <http://www.ipmnet.ru/uniquequip/gfk/#equip>.
32. CR3000x2 Camera. (2019). <https://optronis.com/en/products/cr3000x2-mc/>.
33. GI800 Hydrophones. (2018). <https://all-pribors.ru/opisanie/48796-11-gi800-51670>.
34. Zverev, A. I. (2005). *Handbook of filter synthesis*. Hoboken (NJ), New York: John Wiley & Sons.